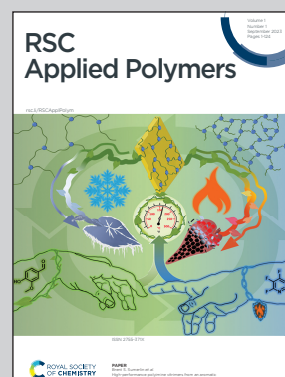Showcasing research from Professor Shao's laboratory, School of Environmental and Biological Engineering, Nanjing University of Science and Technology, Nanjing 210094, P. R. China.

Regulating the preparation of antibacterial poly(amidoxime) for efficient uranium extraction from seawater

Polyacrylonitrile (PAN) contain abound $-C\equiv N$ groups, and is one of hot materials in uranium extraction. However, intermolecular polymerization seriously hindered its application. In this work, a nano-scale antibacterial adsorbent was developed by inhibiting PAN agglutination with K_2FeO_4, and it presents excellent anti-biofouling property and adsorption capability for U(VI) in uranium extraction from seawater.

ROYAL SOCIETY OF CHEMISTRY

rsc.li/RSCApplPolym

Check for updates

Regulating the preparation of antibacterial poly (amidoxime) for efficient uranium extraction from seawater†

Xue Zhang and Dadong Shao [ID] *

Seawater is a huge store of uranium, and the related uranium retraction technology has become a critical step in the sustainable development of nuclear power. For obtaining uranium U(VI) from seawater cheaply and environmentally, we introduced K_2FeO_4 during the polyamidoxime (PAO) preparation process in water to endow PAO with high antibacterial and low agglomeration properties. In this reaction, only water was used as the solvent with the goal of extracting U(VI) from seawater in a low-cost, pollution-free manner. Studies showed that the adsorption of U(VI) on K_2FeO_4@PAO conformed to a pseudo-second-order model, and the maximum adsorption capacity calculated by the Langmuir model was 137 mg g^{-1} at 298 K and pH 8.2. Moreover, K_2FeO_4@PAO showed high selectivity for U(VI) compared with a range of metal ions. K_2FeO_4@PAO also showed good recyclability, and the recovery rate only decreased by 3% after six cycles. In addition, antibacterial experiments indicated that K_2FeO_4@PAO could effectively inhibit the growth of *Escherichia coli* (*E. coli*) and *Vibrio alginolyticus* (*V. alginolyticus*) that are commonly found in seawater.

Introduction

As a low-carbon and efficient energy, the sound development of nuclear power is crucial for a future low-carbon society.[1,2] As the most important nuclear fuel for nuclear power operations, the safe supply of uranium is key to guaranteeing the sustainable development of nuclear power. Traditional terrestrial uranium resources are limited and would be exhausted in few decades. It is thus a worldwide task to explore new uranium resources. As a typical uranium resource, seawater has attracted worldwide attention because an estimated ~4.5 billion tons of U(VI) in seawater can solve the global shortage of uranium.[3,4] There is thus an urgent need to develop appropriate methods and materials for seawater U(VI) extraction.[5–7] Thus far, several technologies have been reported to recover U(VI) from seawater, such as ionic exchange, electrochemical process, co-precipitation, and adsorption method.[8–11] Among them, adsorption has been widely adopted due to its low cost and practicability. However, the complexity of the marine environment, such as very low U(VI) concentration (~3 ppb), presence of many coexisting competing ions, high salinity, and easy biofouling, makes the U(VI) extraction process extre-

mely challenging.[12–14] Other factors, such as the technical economy of the extraction process, also need to be seriously considered. Therefore, it is necessary to develop high-performance materials to improve comprehensive properties of the used adsorbents to enable the economical extraction of U(VI) from seawater.[15]

Polyamidoxime (PAO)-based materials can adsorb U(VI) due to the O and N atoms of PAO having the same distance and lone pair of electrons, and these are thus among the hot materials in U(VI) extraction research. Resulting from polyacrylonitrile's (PAN) low cost, good chemical stability, and easy industrial production, numerous adsorbents select it to prepare PAO-based materials for U(VI) recovery.[16–18] There are many methods for synthesizing PAO in the laboratory. The classic synthesis method is –C≡N amidoximation, which can be divided into homogeneous and heterogeneous processes according to the solvent. The homogeneous method mainly involves the reaction of PAN and NH_2OH in an organic solvent with dimethyl sulfoxide and *N,N'*-dimethyl formamide generally chosen in the laboratory. The heterogeneous method mainly involves the reaction of PAN with NH_2OH in water and methanol/water solutions. Organic solvents are often required in this method, which makes it not only harmful to the environment but also increases the cost of U(VI) recovery, dramatically reducing the competitiveness of PAO in U(VI) extraction. Thus, we considered selecting water as a solvent during the amidoximation process. PAN, as a macromolecule

School of Environmental and Biological Engineering, Nanjing University of Science and Technology, Nanjing 210094, P R China. E-mail: shaodadong@126.com

material, is prone to agglomerate in water, leading to intra-molecular bond accumulation without the reaction of its groups.[19,20] In this work, K_2FeO_4 was adopted to inhibit the aggregation of PAN in water with an aim to obtain a higher conversion rate.

In the U(VI) extraction process, the interaction between U(VI) extraction materials and marine microorganisms should be considered in addition to improving the U(VI) recovery rate and cost.[21,22] Seawater is a very harsh corrosive environment, which is typically characterized by high biological activity, with 10^6 colony-forming units (CFU) per mL level microbes (including bacteria and microalgae) found to exist in seawater. The microbes and their metabolisms affect material surface properties, which can eventually affect the U(VI) extraction performance. Thus, there is a necessity to design a novel adsorbent to achieve an antifouling goal.[15,23,24] The corresponding standard electrode potentials of FeO_4^{2-} both in acid (2.20 V) and alkali (0.72 V) media are higher than the well-known strong oxidant $KMnO_4$ under the same conditions. This strong oxidation ensures the strong bactericidal ability of FeO_4^{2-}. K_2FeO_4 can kill both Gram-positive and Gram-negative bacteria, fungi, viruses, and spores.[25,26] The introduced K_2FeO_4 in PAN can inhibit the corrosion from marine microorganisms.

The structure of a material determines its properties, and ultimately affects its application optimizing the structure of a material is an effective way to enhance its properties and expand its application fields. Herein, we constructed the anti-biofouling nanoscale adsorbent $K_2FeO_4@PAO$ for U(VI) recovery by introducing K_2FeO_4 during the amidoximation method with only water as a solvent (Fig. 1). The added K_2FeO_4 could overcome PAN agglomeration in water, so that PAN could well contact with NH_2OH, which could help realize the economic and environmental recovering of uranium. Meanwhile, the high oxidation ability of K_2FeO_4 could exterminate bacterial. The obtained antibacterial $K_2FeO_4@PAO$ particles exhibited a higher adsorption capacity and better anti-biofouling properties than PAO under the experimental conditions.
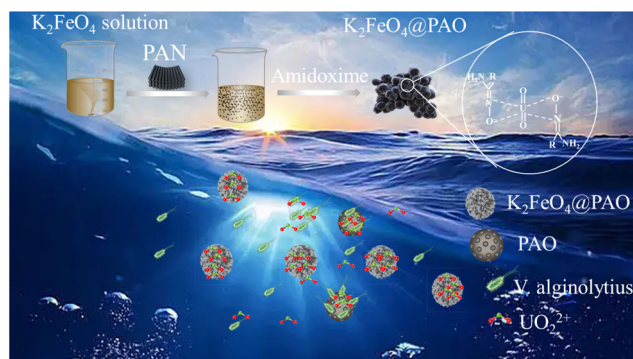
Results and discussion

Characterization

As shown in Fig. S1A and B,† PAN tends to aggregate into large particles and is extremely unstable in aqueous solution, which is detrimental to the conversion of PAN into PAO, and ultimately affects the adsorption capability of PAO. Therefore, K_2FeO_4 was introduced to inhibit the agglomeration of PAN during the amidoximation process in this work. This is a simple way to obtain a high conversion of PAN, which would accelerate the practical application of PAO as a candidate for U(VI) extraction from seawater. As shown in Fig. S1C,† after introducing K_2FeO_4, the obtained PAO-based material could uniformly disperse in aqueous solution and the PAO appearance was improved overall. Given the effect of K_2FeO_4 on the inhibition of PAN particle agglomeration, the obtained PAO morphology may be regulated by K_2FeO_4.

To study the effect of K_2FeO_4 on the PAO surface topologies, the microstructures of PAN and PAO prepared at different conditions were analyzed by SEM (Fig. 2A), with varying the addition amounts of K_2FeO_4 and PAN in the preparation process, as shown in Table 1. The SEM images indicated that the addition of 0.20 g K_2FeO_4 had no significant effect on PAO surface topologies, and the obtained $K_2FeO_4@PAO$ was uniformly dispersed. As the mass of K_2FeO_4 increased, PAN agglomeration became more evident, and eventually, a PAN block was formed. The three reactions include the formation of $-C\equiv N$ from unsaturated amine, the redox reaction between NH_2OH and K_2FeO_4, and the conversion of $-C\equiv N$ to $-C(NH_2)=N-OH$, which restrict and promote each other in water. When the amounts of PAN and NH_2OH were much more than K_2FeO_4, the amidoximation reaction was the primary reaction in solution, and finally, uniform dispersed PAO particles were obtained. When the K_2FeO_4 amount was higher than PAN and
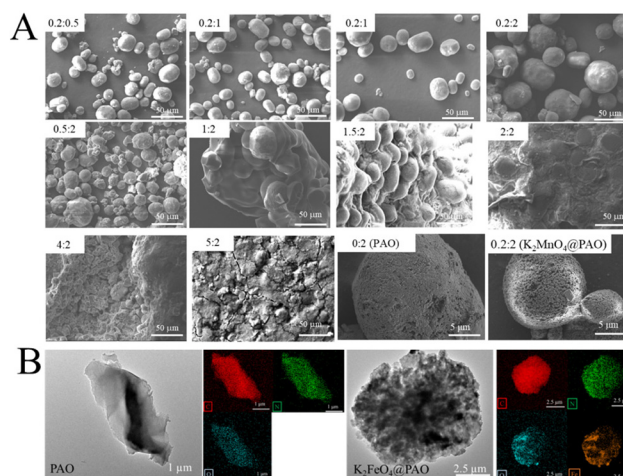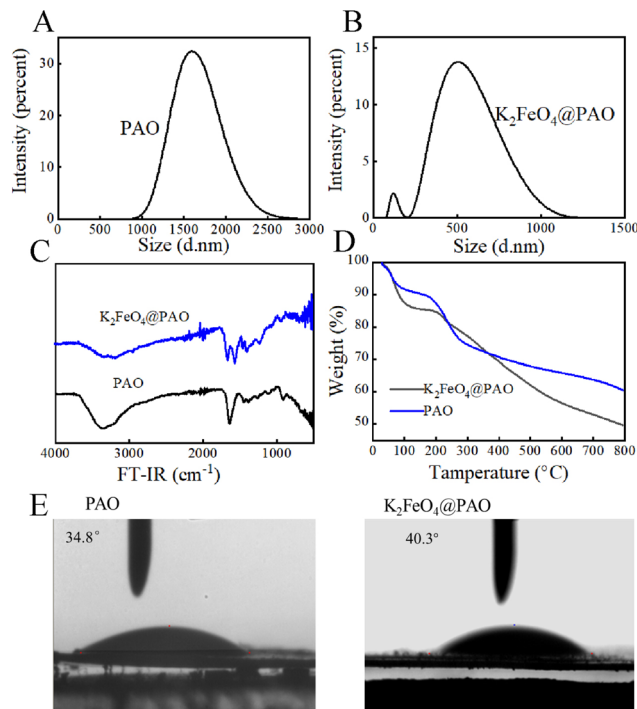

Fig. 1 Scheme for the fabrication and application of $K_2FeO_4@PAO$ in the extraction of U(VI) from seawater.

Fig. 2 SEM images of $K_2FeO_4@PAO$ with different K_2FeO_4 and PAO contents (A) and TEM image and EDS mappings of PAO and $K_2FeO_4@PAO$ (B). The preparation conditions for $K_2FeO_4@PAO$ are shown in Table 1.

© 2023 The Author(s). Published by the Royal Society of Chemistry

RSC Appl. Polym., 2023, **1**, 46–54 | **47**

Table 1 Preparation conditions for K_2FeO_4@PAO

	K_2FeO_4 (g)	PAN (g)	Name
Fixed K_2FeO_4 series	0.20	0.50	0.2 : 0.5
		1.00	0.2 : 1
		1.50	0.2 : 1.5
		2.00	0.2 : 2
Fixed PAN series	0	2.00	0 : 2
	0.50		0.5 : 2
	1.00		1 : 2
	1.50		1.5 : 2
	2.00		2 : 2
	4.00		4 : 2
	5.00		5 : 2

NH_2OH, the solution reaction was dominated by the redox reaction of K_2FeO_4 and NH_2OH, which consumed most of the NH_2OH and made it impossible to complete the conversion of $-C\equiv N$, instead forming $-C\equiv N$ rings on the PAN macromolecular chains and thus creating bulk materials. Besides SEM, TEM was also applied to study the morphologies of PAO and K_2FeO_4@PAO. As shown in Fig. 2B, the single PAO presents a block form, but transformed into nanoscale particles (K_2FeO_4@PAO) after K_2FeO_4 was introduced. It was found that C, N, and O elements were uniformly distributed on PAO and K_2FeO_4@PAO surfaces by the TEM element mapping. Moreover, Fe was evenly distributed on the K_2FeO_4@PAO surface, proving that K_2FeO_4 recombined with PAO successfully. It is considered that the $-C(NH_2)\!=\!N-OH$ unit in K_2FeO_4@PAO is the core of its application in U(VI) extraction. The adsorption capacity of K_2FeO_4@PAO for U(VI) gradually increased with increasing the PAN amount when the K_2FeO_4 amount was fixed at 0.20 g (Fig. S2A†) and decreased with increasing the K_2FeO_4 amount when the PAN amount was set at 2.00 g (Fig. S2B†). Therefore, the K_2FeO_4 amount should be well controlled during the K_2FeO_4@PAO preparation process. The aggregation of PAN could be significantly inhibited, and PAO particles with smaller particle sizes and better adsorption capability could be obtained at the composition of 0.20 g K_2FeO_4 and 2.00 g PAN. This reactant amount was selected in the following experiment.

The effect of K_2FeO_4 on the PAO particle-size distribution was also studied. Dynamic light scattering (DLS) measurements showed that the PAO particle sizes were concentrated around 1600 nm (Fig. 3A). The particle diameter of K_2FeO_4@PAO was reduced ~31% at 500 nm (Fig. 3B) compared with PAO. The introduced K_2FeO_4 could thus inhibit the agglomeration of PAN in water and promote the formation of nano-sized K_2FeO_4@PAO particles. The smaller K_2FeO_4@PAO particle size will help the adsorbent application in the target solution. The Tyndall phenomenon was used to further verify the size of the two particles. Here, if the particle is smaller than the wavelength of incident light, light scattering occurs. In this case, a light wave around the particle is observed and radiates around it, which is called scattered light and the Tyndall phenomenon is the scattering phenomenon of light.

Fig. 3 Size distributions (A and B), FT-IR spectra (C), TGA curves (D), and water contact angles (E) of PAO and K_2FeO_4@PAO.

In terms of the macroscopic performance for the same incident light, if the particles are small, have a larger scattering angle, the scattered light has a weak flood angle, and its brightness is high, then the Tyndall phenomenon is obvious. If the particles are large, have a small scattering angle, the scattered light has a large flood angle, and a low centre brightness, then the Tyndall phenomenon is poor. As shown in Fig. S3,† the light-scattering angle of the particles of K_2FeO_4@PAO was large, the centre brightness was high, the flooding was small, and the Tyndall phenomenon was obvious. However, PAO had a poor particle size uniformity, and the light tended to be scattered by large particles. The light-scattering angle of the particles was small, the flooding area was large, the centre brightness was low, and the Tyndall path was dark.

FT-IR and TGA were used to analyze the effects of K_2FeO_4 on the surface functional groups and thermal stability of PAO. As shown in Fig. 3C, The FT-IR spectra of K_2FeO_4@PAO and PAO were similar. In the K_2FeO_4@PAO spectrum, the peaks of N–H and O–H were at 3500–3000 cm^{-1}, the peak of $-C\equiv N$ was at ~1668 cm^{-1}, and the characteristic peak of N–O was at ~932 cm^{-1}, which were all consistent with the PAO infrared spectrum. Fig. 3D shows the TGA curves of PAO and K_2FeO_4@PAO. The first ~4% weight losses of PAO and K_2FeO_4@PAO could be assigned to moisture loss. PAO and K_2FeO_4@PAO showed good thermal stability at 100–200 °C. The second weight loss at 200–500 °C was related to the cyclization dehydrogenation of PAO. PAO and K_2FeO_4@PAO then underwent severe oxidative cleavage at 500–700 °C.[19]

Static contact-angle experiments were used to quantify the surface hydrophilic property of PAO and K_2FeO_4@PAO. Before the test, each powder material was pressed into a tablet with a tablet press and the pressure of 20 MPa was maintained for 40 s. During the contact-angle measurement, 2 μL ultrapure water was injected for each test. Each sample was tested three times, and every test used a new sample to exclude residual effects. The results of the three tests are shown in Fig. 3E, whereby the average contact angles of PAO and K_2FeO_4@PAO were 34.8° and 40.3°, respectively. The lower water contact angles of PAO and K_2FeO_4@PAO indicated they both have good hydrophilicity, which would benefit their application in aqueous solution.

XPS was used to infer the binding states of the atoms and the electron distribution in K_2FeO_4@PAO and PAO by measuring the chemical shift of electrons in their layers (Fig. 4A). The high resolution of Fe 2p in the K_2FeO_4@PAO spectrum revealed the characteristic Fe 2p3/2 and Fe 2p1/2 [27–29] of Fe signals located at 711.8 and 724.7 eV, respectively (Fig. S4†). A new peak appeared at ~390 eV (Fig. S5†) related to XPS U 4f[4] after U(VI) adsorption, revealing the high enrichment of U(VI) on PAO and K_2FeO_4@PAO surfaces. The XPS peaks of O 1s, N 1s, and C 1s were located at ~532, ~400, and ~285 eV, respectively. The C 1s spectra (Table S1† and Fig. 4B) could be divided into five components at 284.6 ± 0.1, 285.3 ± 0.1, 286.4 ± 0.1, 287.4 ± 0.1, and 288.6 ± 0.1 eV corresponding to –C≡N, C–C, C–OH and –C(NH₂)=NOH, –C=O, and –COO⁻ groups of PAO and K_2FeO_4@PAO surfaces, respectively. [30,31] As indicated in the N 1s spectra (Fig. 4C and Table S2†), the characteristic peaks with binding energies at 398.7 ± 0.1, 399.3 ± 0.1, and 400.5 ± 0.1 eV were attributed to the –C≡N, N–H, and –C(NH₂)=NOH bonds, respectively. [31,32] The three fitting peaks in the O 1s spectra (Fig. 4D and Table S3†) belonged to –COO⁻ (531.2 ± 0.1 eV), C=O (532.3 ± 0.1 eV), and –OH (533.4 ± 0.1 eV), respectively. [33,34] The XPS results showed that the chemical environments of PAO and K_2FeO_4@PAO were

similar to each other, revealing that K_2FeO_4 did not affect PAO's chemical properties.

Adsorption performance of K_2FeO_4@PAO

The solution pH can affect the forms of U(VI) existing in solution and on the adsorbent surface, therefore affecting the U(VI) adsorption behaviours. [35] Fig. 5A shows that the U(VI) extraction capacity of K_2FeO_4@PAO displayed an increasing trend at pH 2–5. UO_2^{2+} was the dominant form of U(VI) at pH < 4, and K_2FeO_4@PAO was positive due to protonation. Electrostatic repulsion would lead to a poor recovery effect for K_2FeO_4@PAO to U(VI). At pH 4.0–6.0, K_2FeO_4@PAO surface was gradually deprotonated and the electrostatic attraction of the solution-dominant positively charged U(VI) species was enhanced, resulting in increased U(VI) adsorption on K_2FeO_4@PAO. The U(VI) uptake decreased when the pH value increased from 6.0 to 9.0. The main reason for this phenomenon was that the negatively charged U(VI) species was the dominant substance, and so the adsorption capacity of K_2FeO_4@PAO for U(VI) was inhibited by electrostatic repulsion with the pH increasing. The maximum adsorption capacity of K_2FeO_4@PAO (17.1 mg g⁻¹) was obtained at pH ~ 5.0. The higher maximum adsorption capacity of K_2FeO_4@PAO over PAO illustrated that nano-sized K_2FeO_4@PAO favours U(VI) extraction.

The adsorption performances of K_2FeO_4@PAO at different contact times were also studied. U(VI) adsorption on PAO and K_2FeO_4@PAO rose sharply in the first 2 h, and then increased slowly with further increasing the reaction time (Fig. 5B), reaching equilibrium within 8 h. The adsorption kinetics were analyzed by pseudo-first-order ($q_t = q_e \times (1 - \exp(-k_1 t))$, where q_e and q_t (mg g⁻¹) are the adsorbed amounts of U(VI) at equilibrium time and time t (h), respectively, and $k_1 t$ (1 h⁻¹) is the pseudo-first-order kinetic constant) and pseudo-second-order
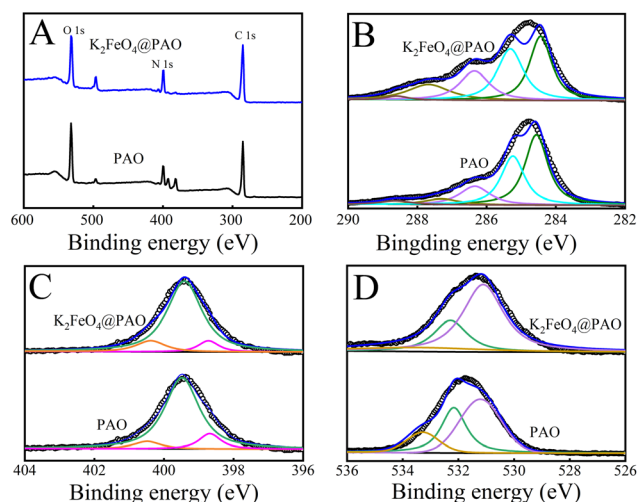

Fig. 4 XPS survey (A), C 1s (B), N 1s (C), and O 1s (D) spectra of K_2FeO_4@PAO and PAO.

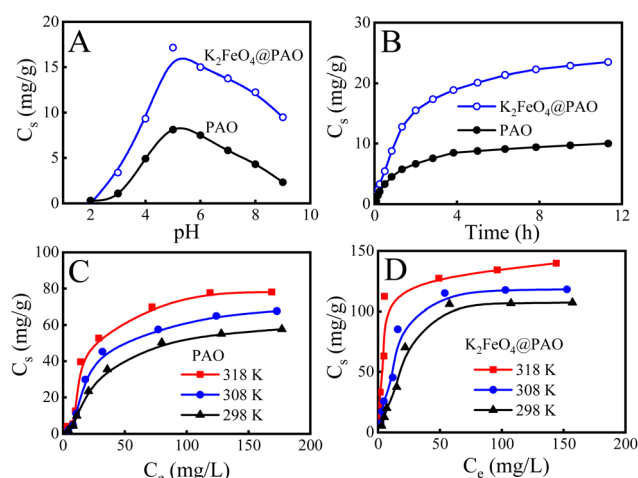**Fig. 5** Effects of pH (A), contact time (B), adsorption isotherms, and reaction temperature on the adsorption of U(VI) on PAO (C) and K_2FeO_4@PAO (D) from solution. m = 0.02 g, V = 50 mL, I = 0.1 mol L⁻¹ NaCl. (A) T = 298 ± 1 K, contact time: 24 h, [U(VI)]$_{initial}$ = 10.0 mg L⁻¹. (B) T = 298 ± 1 K, pH = 8.2 ± 0.1, C[U(VI)]$_{initial}$ = 20.0 mg L⁻¹. (C and D) pH = 8.2 ± 0.1, contact time: 24 h.

© 2023 The Author(s). Published by the Royal Society of Chemistry

RSC Appl. Polym., 2023, **1**, 46–54 | **49**

($q_t = q_e \times t/(1/(K' \times q_e) + t)$, where K' (g (mg h)$^{-1}$) is the pseudo-second-order kinetic constant) models.[36,37] The relevant these parameters coefficients are generalized in Table S4.† The adsorption process of U(VI) by K$_2$FeO$_4$@PAO and PAO conformed to the pseudo-second-order model and chemisorption was the primary adsorption mode for U(VI) adsorption on K$_2$FeO$_4$@PAO and on PAO. According to the relevant results of the pseudo-second-order model, the maximum adsorption capacities of U(VI) on K$_2$FeO$_4$@PAO and PAO were 26.9 and 10.9 mg g^{-1} at pH 8.2 and 298 K, respectively.

Given the above excellent U(VI) recovery performance of K$_2$FeO$_4$@PAO, its effect for U(VI) recovery in various environmental solutions was also studied. As shown in Table 2, K$_2$FeO$_4$@PAO could effectively extract most U(VI) from this complex system. Therefore, the real application of K$_2$FeO$_4$@PAO in extraction U(VI) from seawater was performed, and seawater was prepared with sea salt. We found that K$_2$FeO$_4$@PAO could effective uptake ~57% of 5 mg L^{-1} U(VI) from seawater. Experimental results further confirmed the high efficiency of K$_2$FeO$_4$@PAO in the extraction of U(VI) from seawater.

Adsorption isotherms was used to depict the adsorption capacities of K$_2$FeO$_4$@PAO and PAO at three different temperatures (i.e. 298, 308, and 318 K). As shown in Fig. 5C and D, with increasing the U(VI) initial concentration and temperature, the adsorption capacities of K$_2$FeO$_4$@PAO and PAO for U(VI) increased. Langmuir ($C_s = b \times C_{s,max} \times C_{eq}/(1 + b \times C_{eq})$, where C_{eq} is the equilibrium concentration of U(VI) after adsorption, $C_{s,max}$ (mg g^{-1}) and b (L mg^{-1}) are the maximum adsorption capability of the adsorbent and the Langmuir constant, respectively) and Freundlich ($C_s = K \times C_e^{1/n}$, K (mg g^{-1}) and $1/n$ are the constants indicative of the adsorption capability and intensity, respectively) models were used to fit the experimental data, and the mechanism of the adsorption process is discussed.[36,37] According to the R^2 values in Table S5,† the Langmuir isotherm model could better describe the experimental data, suggesting there was no interaction between the adsorption sites, and the U(VI) adsorption process on K$_2$FeO$_4$@PAO was a monolayer adsorption. The $C_{s,max}$ value K$_2$FeO$_4$@PAO for U(VI) at pH 8.2 and 298 K was calculated to be 137 mg g^{-1}.

According to the adsorption results, the adsorption capacity of PAO prepared in water was lower than that reported when prepared in organic reagents.[38–40] From the perspective of economic cost and environmental protection, obtaining PAO in water is more conducive to the long-term development of PAN as a material for extracting U(VI) from seawater. More importantly, the PAO's preparation in water has not been reported yet. PAN is widely used in U(VI) recovery, mainly because its surface contains a large number of –C≡N groups, which can be converted into –C(NH$_2$)N=OH by chemical reaction with NH$_2$OH in solution and –C(NH$_2$)N=OH can coordinate with U(VI) to recover uranium. However, one cannot ignore that PAN is easy to agglomerate and most –C≡N is not reacted with NH$_2$OH in water, resulting in PAO having a low adsorption capacity for U(VI). Here, K$_2$FeO$_4$@PAO nanoparticles were obtained after K$_2$FeO$_4$ was introduced into the PAN transformation process. Compared with PAO, the adsorption capacity of K$_2$FeO$_4$@PAO was significantly increased, indicating that PAN reacted more fully with NH$_2$OH and the amount of –C(NH$_2$)N=OH on its surface increased.

The relevant thermodynamic parameters,[41] standard enthalpy change ($\Delta H°$), standard Gibbs free energy change ($\Delta G°$), and entropy change ($\Delta S°$) of K$_2$FeO$_4$@PAO and PAO for U(VI) adsorption at three different temperatures (i.e. 298, 308, and 318 K) were investigated and are discussed, and the results are shown in Table S6.† The energy released or adsorbed in the chemical reaction process can be expressed by heat, called the heat of reaction, also known as the "enthalpy change" ($\Delta H°$). $\Delta H° > 0$ means that the adsorption of U(VI) on K$_2$FeO$_4$@PAO and PAO surfaces is an endothermic process, which is consistent with the improved U(VI) adsorption at higher reaction temperature. For a chemical reaction, the $\Delta G°$ value determines the reaction direction. The negative $\Delta G°$ value indicated that the adsorption of U(VI) on K$_2$FeO$_4$@PAO and PAO is a spontaneous process, which also confirmed the strong affinity between –C(NH$_2$)N=OH and U(VI).

To evaluate the stability of K$_2$FeO$_4$@PAO, the desorption–regeneration properties of K$_2$FeO$_4$@PAO were studied. Different concentrations and solvents were used to eluate K$_2$FeO$_4$@PAO. First, 0.5 mol L^{-1} HCl, HNO$_3$, NaOH, and Na$_2$CO$_3$ were selected as eluting agents for the desorption of U(VI) from the K$_2$FeO$_4$@PAO surface. As shown in Fig. S6,† Na$_2$CO$_3$ showed the best resolution rate at 99%. Different concentrations (0.1–1 mol L^{-1}) of Na$_2$CO$_3$ solution were used to eluate the K$_2$FeO$_4$@PAO. The elution results are shown in Fig. 6A, where it can be seen that the elution rate gradually increased with the increase in Na$_2$CO$_3$ concentration. When the Na$_2$CO$_3$ concentration reached 0.5 mol L^{-1}, the solution elution rate could reach almost 100%, so 0.5 mol L^{-1} Na$_2$CO$_3$ solution could achieve effectively regenerate K$_2$FeO$_4$@PAO. The adsorption capability of the regenerated K$_2$FeO$_4$@PAO for U(VI) is shown in Fig. 6B. The adsorption capacity of K$_2$FeO$_4$@PAO

Table 2 Selected results of U(VI) adsorption on K$_2$FeO$_4$@PAO. m/V = 0.40 g L^{-1}, T = 298 ± 1 K, contact time: 24 h, pH 8.2 ± 0.1

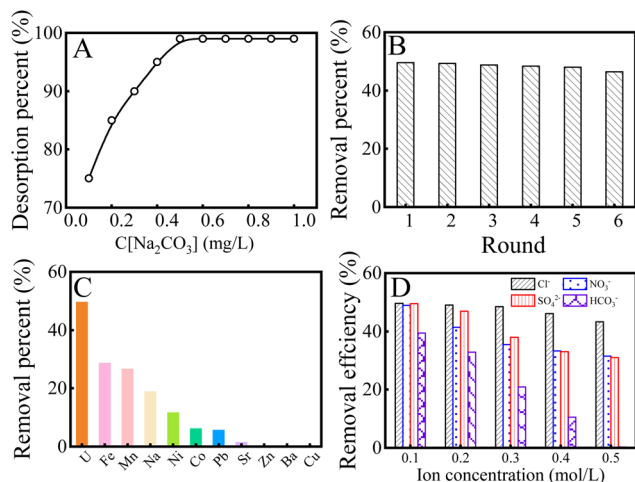| Sample	C[U(VI)] (mg L^{-1})		
	Initial	Final	Adsorption (%)
Diluted U(VI) sloution	20	10.62	46.90
	15	7.07	52.87
	10	5.04	49.60
	5	2.85	43.00
Running water	20	13.39	33.05
	15	8.65	42.33
	10	6.40	36.00
	5	2.87	42.60
Seawater	20	14.51	27.45
	15	8.78	41.47
	10	5.78	42.20
	5	2.17	56.60

Fig. 6 Effect of Na_2CO_3 concentration on the desorption of U(vi) from K_2FeO_4@PAO (A); recycling of K_2FeO_4@PAO in the extraction of U(vi) from solution (B); comparison of K_2FeO_4@PAO enrichment performance for 10 mg L^{-1} U(vi) and heavy metal ions (C); U(vi) removal efficiency for K_2FeO_4@PAO with the coexistence of different anions (D). I = 0.1 mol L^{-1} NaCl, T = 298 $\pm$ 1 K, contact time: 24 h. $C[U(vi)]_{initial}$ = 10.0 mg L^{-1}, m = 0.02 g, V = 50 mL, pH = 8.2 $\pm$ 0.1.

only decreased by 3% after its regeneration and reuse six times.

Based on the complex compositions of seawater, the coexistence of ions in seawater can affect the U(vi) adsorption. With various metal ions coexisting in seawater (such as Na(i), Ba(ii), Sr(ii), Ni(ii), Co(ii), Zn(ii), Cu(ii), Mn(ii), Pb(ii), and Fe(iii)), ICP-MS was used to detect the concentration of each ion and then to evaluate the selectivity of K_2FeO_4@PAO for U(vi). As depicted in Fig. 6C, the adsorption capacity of K_2FeO_4@PAO for U(vi) was higher than that of the other ions, indicating that K_2FeO_4@PAO had excellent selective adsorption capacity for U(vi) in the coexistence ion system. The recovery of U(vi) from anionic solutions was also investigated for K_2FeO_4@PAO. As shown in Fig. 6D, with the increase in ion concentration, the influence of HCO_3^- on U(vi) recovery was undeniable due to the formation of new U(vi) species. In natural seawater, the concentration of various anions is far lower than 0.1 mol L^{-1}, which means that anions have little effect on recycling U(vi).[42] K_2FeO_4@PAO was obtained by introducing K_2FeO_4 into PAN to inhibit PAN agglomeration in water. The overall structure and morphology of the adsorbent were optimized. The particle size of K_2FeO_4@PAO can reach the nanometre scale, and it can be evenly dispersed in solution, so that the adsorbent can better contact with U(vi) and promote the occurrence of chemical reactions. The introduced K_2FeO_4 did not damage the stability and selectivity of PAO. As we expected, the adsorption capability of K_2FeO_4@PAO was much higher than PAO in various U(vi) solutions. In K_2FeO_4@PAO, PAO ensures the excellent selectivity of K_2FeO_4@PAO for U(vi), and the nanoscale particle size enables K_2FeO_4@PAO to fully react with U(vi) in solution, ultimately ensuring that K_2FeO_4@PAO has better adsorption effect on U(vi) than other ions in complex systems.

Furthermore, K_2FeO_4@PAO also showed good cycling and selectivity for U(vi). In summary, K_2FeO_4@PAO can not only reduce the cost of the PAO preparation process and make the process greener, but can also further optimize the surface structure of the PAO and improve its adsorption properties in a variety of environments.

Antibacterial activity of K_2FeO_4@PAO

Many marine microorganisms in seawater will accumulate on the surface of materials, resulting in the biological contamination of materials, which will lead to materials corrosion and finally affect the U(vi) adsorption performance. Conventionally obtained PAO powders have no ability to resist biological fouling and often need to work synergistically with other antibacterial materials in the field of anti-biological fouling U(vi) extraction from seawater. As is well known, K_2FeO_4 presents excellent properties in decontamination, off-colour, and flocculation applications *etc.* Researchers have also found that the strong oxidation of K_2FeO_4 can destroy bacterial structures (such as cell walls and cell membranes) and suppress the reproduction of bacteria.[24,25] Combining K_2FeO_4 with PAO can be expected to break through the inhibition of PAO adsorption by marine bacteria and maintain good U(vi) recovery performance in bacteria-containing solutions. *Vibrio marine* is a kind of bacteria commonly living in the ocean. Here, we took *V. alginolyticus* as an example to investigate the effects of marine microorganisms on the U(vi) recovery performance by PAO and K_2FeO_4@PAO. We adjusted the *V. alginolyticus* concentration to 1.0×10^6 CFU mL^{-1} (close to its concentration in offshore areas) and balanced this with PAO and K_2FeO_4@PAO for 24 h. As shown in Fig. 7A, *V. alginolyticus* resulted in severe biological contamination and significantly decreased the adsorption capacity compared with the samples without bac-
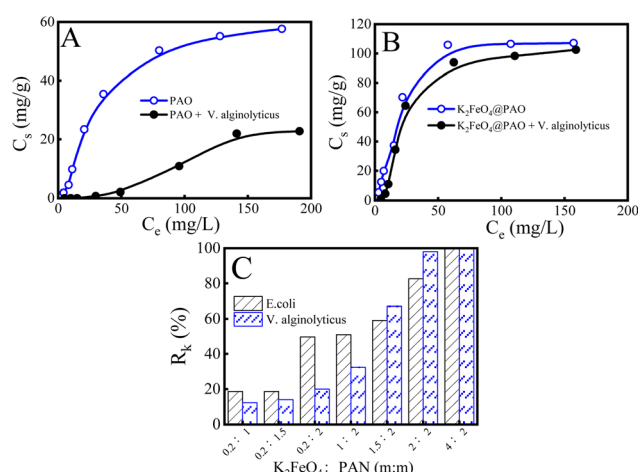

Fig. 7 Adsorption of U(vi) by PAO (A) and K_2FeO_4@PAO (B) in solutions of different concentrations. m = 0.02 g, V = 50 mL, I = 0.1 mol L^{-1} NaCl. T = 298 $\pm$ 1 K, pH = 8.2 $\pm$ 0.1, contact time: 24 h; bactericidal rates against *E. coli* and *V. alginolyticus* of different particles (C). The K_2FeO_4@PAO materials were named according to the used amounts of K_2FeO_4 and PAN (Table 1).

© 2023 The Author(s). Published by the Royal Society of Chemistry

RSC Appl. Polym., 2023, **1**, 46–54 | **51**

teria. These results indicated that biofouling has a significant effect on PAO-based materials. Unlike PAO, the recovery capability of K_2FeO_4@PAO for U(VI) did not significantly decrease compared with the data results for tests performed under sterile conditions, indicating that the K_2FeO_4 ensured K_2FeO_4@PAO presented excellent anti-biofouling properties (Fig. 7B). Therefore, we studied the effect of the K_2FeO_4 and PAO contents on the anti-biofouling properties of K_2FeO_4@PAO, using two Gram-negative bacteria (*E. coli* and *V. alginolyticus*). Fig. S7† shows the change in colonies of *E. coli* and *V. alginolyticus* on agar plates at different conditions. Fig. 7C exhibits the bactericidal rates calculated by the Petri dish counting method to quantitatively analyze different materials antibacterial properties. The results showed that K_2FeO_4 is critical for the anti-biofouling properties of K_2FeO_4@PAO for *E. coli* and *V. alginolyticus*, and the anti-biofouling performance increased with increasing the K_2FeO_4 content in K_2FeO_4@PAO. K_2FeO_4@PAO could kill almost all *E. coli* and *V. alginolyticus* when the K_2FeO_4 dosage was increased to 4.0 g. The introduced K_2FeO_4 not only promoted formatting PAO with good recovery performance for U(VI), but also directly endowed the PAO with antibacterial properties to maintain good recovery for U(VI) in bacterial-containing solutions.

Conclusions

Considering the limitation of PAO as a single material for U(VI) extraction from seawater, we further optimized the structure of PAN during the conversion of PAN into PAO to further enable the application of PAO to be used for multiple relationships. The results showed that fine control of K_2FeO_4 dosage during the preparation process can effectively enhance the anti-biofouling property and adsorption capability of the PAO-based material (K_2FeO_4@PAO) for extracting U(VI) from seawater. K_2FeO_4@PAO displayed good adsorption and circulatory capacities under laboratory conditions. K_2FeO_4@PAO also showed remarkable selectivity for U(VI) against multiple coexisting metal ions. Due to the K_2FeO_4 effect, K_2FeO_4@PAO exhibited excellent anti-biofouling property, and could kill almost all *E. coli* and *V. alginolyticus*. In summary, research attempts to convert PAN into PAO in water and inhibit PAN agglomeration, improve the conversion rate of surface functional groups, improve its U(VI) adsorption capacity, and confer antibacterial properties will promote the further development of low-cost, pollution-free, and biofouling resistant U(VI) extraction materials from seawater.

Experimental section

Synthesis of K_2FeO_4@PAO

Two series of K_2FeO_4@PAO materials with different mass ratios (Table 1) were prepared by regulating PAN and K_2FeO_4. Specific amounts of K_2FeO_4 and PAN powder, 3.20 g

$NH_2OH \cdot HCl$, and 1.75 g NaOH were added into 20 mL degassed water. The solution was reacted at 75 °C for 6 h. After washing with de-gassed water, the K_2FeO_4@PAO materials were vacuum dried at 75 °C. To evaluate the effect of K_2FeO_4, PAO was also prepared by the same method.

Synthesis of PAO in methanol/water solution

NH_2OH solution was prepared by dissolving 4.0 g $NH_2OH \cdot HCl$ in 50 mL methanol/water (4 : 1, V/V) solution, and the pH was adjusted to ~7.0 with NaOH under stirring condition. Then, 2.0 g PAN powder was added to the solution. Amidoximation reactions were performed at 75 °C for 6 h in a 100 mL glass flask under nitrogen and electromagnetic stirring condition. The resulting material was repeatedly washed with methanol/water (4 : 1, V/V) to remove the residual NH_2OH, and then vacuum dried at 50 °C.

Synthesis of PAO in H_2O

After 3.2 g $NH_2OH \cdot HCl$ was dissolved in 20 mL de-gassed water, NaOH was slowly added to pH ~ 7.0 under stirring condition. Then, 2.0 g PAN powder was added and reacted at 75 °C for 6 h. The resulting material was washed with de-gassed water, and vacuum dried at 50 °C.

Characterization

Scanning electron microscopy was adopted to analyze the morphology of the particles (SEM, FEI Quanta 250 FEG) and transmission electron microscopy (TEM, FEI Tecnai G2 F20) was used to obtain the morphology of the particles. FT-IR spectroscopy was mounted on a Bruker Tensor II system with a platinum ATR instrument at room temperature. Thermogravimetric analysis (TGA, TGA 5500) was performed from room temperature to 800 °C under N_2 atmosphere at a uniform heating rate of 10 °C min^{-1}. X-Ray photoelectron spectroscopy (XPS) measurements were obtained with an ESCALab220i-XL surface microanalysis system (VG Scientific) equipped with an Al Kα ($h\lambda$ = 1486.6 eV) source at a chamber pressure of 3×10^{-9} mbar. The surface charging effects were corrected with the C 1s peak at 284.4 eV as a reference. Dynamic light scattering (DLS) measurements were used to measure the distribution of particles. DLS was operated on a Malvern Instruments Zetasizer operated in the backscatter (173°) mode. The PAO and K_2FeO_4@PAO were dispersed in methanol to prepare 250 mg L^{-1} and 500 mg L^{-1} sample slurries. A 10 mm sample pool was used for the measurements. The hydrophilicity of the adsorbents was determined by the dynamic contact angle of pure water droplets on a solid surface with a contact angle meter (JC200d Zhongchen Digital Technology, China).

Batch adsorption experiments

The adsorption capabilities of K_2FeO_4@PAO for U(VI) were studied by batch adsorption technique, with $UO_2(NO_3)_2 \cdot 6H_2O$ (>99% purity) used as the U(VI) source. U(VI) stock solution was prepared from $UO_2(NO_3)_2 \cdot 6H_2O$ (>99% purity). Different concentrations of U(VI) sample solutions were prepared from the

52 | *RSC Appl. Polym.*, 2023, **1**, 46–54

© 2023 The Author(s). Published by the Royal Society of Chemistry

stock solution. Briefly, after K$_2$FeO$_4$@PAO and PAO were pre-equilibrated with NaCl for 24 h, a solution containing U(VI) diluted to a certain concentration with ultrapure water was added. The salinity of seawater is ∼3.5%, and most of it is NaCl. Because of the considerable amount of water used, the adsorbent must be competent for normal seawater values and salinity conditions. The equilibrium of the adsorbent in NaCl solution lays the foundation for K$_2$FeO$_4$@PAO for U(VI) extraction from seawater. The solution pH values were adjusted by adding 0.1 mol L^{-1} NaOH or HCl. After shaking for the desired time in a thermostatic oscillation incubator, the suspension was filtered with a 0.22 μm needle filter. The final U(VI) concentration in the supernatant was measured by inductively coupled plasma mass spectrometry (ICP-MS, Thermo Scientific X-Series II, λ = 358.8 nm). The adsorption capacity of U(VI) was calculated as follows:

$$C_s = (C_0 - C_e) \times \frac{v}{m} \quad (1)$$

$$R = \frac{C_0 - C_e}{C_0} \times 100\% \quad (2)$$

where V (L) is the volume of solution; C_0 (mg L^{-1}) refers to the original U(VI) concentration; C_s stands for the adsorption capacity, m (g) represents the mass of adsorbent; R stands for the removal percentage; and C_e (mg L^{-1}) is expressed as the equilibrium U(VI) concentration.

Desorption of U(VI) from K$_2$FeO$_4$@PAO

Here, 0.5 mol L^{-1} Na$_2$CO$_3$ was used as the eluting agent to study the desorption of U(VI) from the K$_2$FeO$_4$@PAO surface. Briefly, 0.02 g U(VI)-laden K$_2$FeO$_4$@PAO was immersed in 50 mL 0.5 mol L^{-1} Na$_2$CO$_3$ and shaken at 200 rpm for 24 h. The regenerated K$_2$FeO$_4$@PAO was washed with de-gassed water and vacuum dried at 50 °C.

Antibacterial property

The two kinds of Gram-negative bacteria *E. coli* and *V. alginolyticus* were chosen to verify the antibacterial properties of K$_2$FeO$_4$@PAO. The bacteria were severally cultured in Luria–Bertani (LB) medium and shaken at 37 °C for 12 h. The resulting bacterial suspension was subsequently centrifuged at 10 000 rpm for 10 min. The obtained bacterial precipitate was diluted by sterile physiological saline and the cell density was adjusted to ∼1.0 × 10^6 CFU mL^{-1}. Next, 0.02 g K$_2$FeO$_4$@PAO and 50 mL diluted bacterial solution at 37 °C were incubated for 24 h to determine the antibacterial activity. The cultured bacterial solution (0.1 mL) was taken out and diluted and spread on an LB nutrient agar plate, followed by cultivation at 37 °C for 24 h.

Effect of biofouling on U(VI) adsorption

To obtain the target compositions, the adsorbents (K$_2$FeO$_4$@PAO) and NaCl were pre-reacted for 24 h at first; and then deionized water, U(VI), and exponential growth phase *V. alginolyticus* were injected, finally adjusting the suspension

pH. After reacting for 24 h, the suspensions were centrifugated at 9000 rpm for 30 min at 25 °C, and then filtered. Except for specific evaluations, the reaction temperature, time, m/V, pH, and ionic strength were 298 ± 1 K, 24 h, 0.04 g L^{-1}, 8.2 ± 0.1, and 0.10 mol L^{-1} NaCl, respectively. The final U(VI) concentrations were analyzed by inductively coupled plasma mass spectrometry (ICP-MS, Thermo Scientific X-Series II, λ = 358.8 nm).

Conflicts of interest

There are no conflicts to declare.

Acknowledgements

References

1 Z. H. Liu, S. Shinde, S. Xie, N. Hao, F. Lin, C. G. Yoo, A. J. Regaukes and J. S. Yuan, *Sustainable Energy Fuels*, 2019, **3**, 2024–2037.

2 X. Luo, J. Zhang, J. Tao, X. Wang, S. Zhao, Z. Chen, S. Liu, J. Li and S. Li, *Chem. Eng. J.*, 2021, **416**, 129486.

3 R. Yu, Y. Lu, X. Zhang, W. Chen, X. Chen and L. Li, *Desalination*, 2022, **539**, 115965.

4 N. Li, P. Gao, H. Chen, F. Li and Z. Wang, *Chemosphere*, 2022, **287**, 116153.

5 Z. Mi, D. Zhang, J. Wang, S. Bi, J. Liu, X. Gao, D. Zhang, Y. Jiang, Z. Li, Y. Zhu and Z. Liu, *New J. Chem.*, 2022, **46**, 6296–6306.

6 X. Chen, C. Wan, R. Yu, L. Meng, D. Wang, T. Duan and L. Li, *Desalination*, 2020, **486**, 114447.

7 C. Liu, P. C. Hsu, J. Xie, J. Zhao, T. Wu and H. Wang, *Nat. Energy*, 2017, **2**, 17007–17014.

8 F. Chi, S. Zhang, J. Wen, J. Xiong and S. Hu, *Ind. Eng. Chem. Res.*, 2018, **57**, 8078–8084.

9 X. Liu, H. Liu, H. Ma, C. Cao, M. Yu, Z. Wang, B. Deng, M. Wang and J. Li, *Ind. Eng. Chem. Res.*, 2012, **51**, 15089–15095.

10 X. Lu, D. Zhang, A. T. Reda, C. Liu, Z. Yang, S. Guo, S. Xiao and Y. Ouyang, *Ind. Eng. Chem. Res.*, 2017, **56**, 11936–11947.

11 F. Ma, B. Dong, Y. Gui, M. Cao, L. Han, C. Jiao, H. Lv, J. Hou and Y. Xue, *Ind. Eng. Chem. Res.*, 2018, **57**, 17384–17393.

12 F. Endrizzi and L. F. Rao, *Chem. – Eur. J.*, 2014, **20**, 14499–14506.

13 S. Shi, B. Li, Y. Qian, P. Mei and N. Wan, *Chem. Eng. J.*, 2020, **397**, 9–17.

14 C. Ma, J. Gao, D. Wang, Y. Yuan, J. Wen, B. Yan, S. Zhao, X. Zhao, Y. Sun, X. Wang and N. Wang, *Adv. Sci.*, 2019, **6**, 1900085.

© 2023 The Author(s). Published by the Royal Society of Chemistry

RSC Appl. Polym., 2023, **1**, 46–54 | **53**

15 F. Endrizzi, C. J. Leggett and L. Rao, *Ind. Eng. Chem. Res.*, 2016, **55**, 4249–4256.

16 J. Zhang, J. Ma, G. Jiao, K. Liu, R. Cui, S. Zhai and R. Sun, *Desalination*, 2023, **548**, 116243.

17 G. Jiao, J. Ma, J. Zhang, S. Zhai and R. Sun, *Carbohydr. Polym.*, 2023, **300**, 120244.

18 X. Chen, Y. Lin, W. Li, G. Zhang, Y. Wang, J. Ma, Z. Meng, S. Wu, S. Wang, X. Zhang and H. Pang, *Sustainable Mater. Technol.*, 2022, **34**, e00521.

19 D. Shao, G. Hou, F. Chi, X. Lu and X. Ren, *RSC Adv.*, 2021, **11**, 1909–1915.

20 G. Wang, C. Lu, T. Sun and Y. Li, *J. Appl. Polym. Sci.*, 2022, **139**, 52129.

21 C. Bi, C. Zhang, W. Xu, F. Ma, L. Zhu, R. Zhu, Q. Qi, L. Liu, J. Bai and H. Dong, *Desalination*, 2023, **545**, 116169.

22 C. Zhang, Y. Song, Q. He, F. Wang, S. Zhan and F. Zhou, *J. Environ. Chem. Eng.*, 2021, **9**, 105973.

23 W. Sun, L. Feng, J. Zhang, K. Lin, H. Wang, B. Yan, T. Feng, M. Cao, T. Liu, Y. Yuan and N. Wang, *Adv. Sci.*, 2022, **9**, 2105008.

24 Q. Chen, X. Xue, Y. Liu, A. Guo, K. Chen, J. Yin, F. Yu, H. Zhu and X. Guo, *J. Hazard. Mater.*, 2022, **438**, 129524.

25 M. Thomas, P. Drzewicz, A. Więckol-Ryk and K. Schwochau, *Environ. Sci. Pollut. Res.*, 2022, **29**, 8514–8524.

26 V. G. Petrov, Y. D. Perfiliev, S. K. Dedushenko, T. S. Kuchinskay and S. N. Kalmykov, *J. Radioanal. Nucl. Chem.*, 2016, **310**, 347–352.

27 N. Wang, L. Tan, R. Zhang, Q. Zhao and H. Wang, *Sci. Total Environ.*, 2020, **726**, 138541.

28 Z. Viktor, L. Wang and J. Ma, *J. Hazard. Mater.*, 2020, **384**, 121264.

29 Y. Tan, Z. Xu, L. He and H. Li, *J. Energy Storage*, 2022, **52**, 104889.

30 D. Wang, J. Song, J. Wen, Y. Yuan, Z. Liu, S. Lin, H. Wang, H. Wang, S. Zhao, X. Zhao, M. Fang, M. Lei, B. Li, N. Wang, X. Wang and H. Wu, *Adv. Energy Mater.*, 2018, **8**, 1802607.

31 J. Zeng, H. Zhang, Y. Sui, N. Hu, D. Ding, F. Wang, J. Xue and Y. Wang, *Ind. Eng. Chem. Res.*, 2017, **56**, 5021–5032.

32 W. Li, Q. Liu, J. Liu, H. Zhang, R. Li, Z. Li, X. Jing and J. Wang, *Appl. Surf. Sci.*, 2017, **403**, 378–388.

33 D. Shao, X. Wang, X. Ren, S. Hua, J. Wen, Z. Tan, J. Xiong, A. M. Asiric and H. M. Marwani, *J. Ind. Eng. Chem.*, 2018, **67**, 380–387.

34 D. Shao, X. Liu, T. Hayat, J. Li and X. Ren, *J. Radioanal. Nucl. Chem.*, 2019, **319**, 379–386.

35 C. W. Abney, R. T. Mayes, T. Saito and S. Dai, *Chem. Rev.*, 2017, **117**, 13935–14013.

36 H. Wang, T. Xu, B. Zheng, M. Cao, F. Gao, G. Zhou, C. Ma, J. Dang, W. Yao, K. Wu, T. Liu, Y. Yuan, Q. Fu and N. Wang, *J. Hazard. Mater.*, 2022, **433**, 128789.

37 N. Li, J. Wu, R. Su, N. Zhang, J. Zhao and Z. Wang, *Desalination*, 2023, **545**, 116153.

38 Y. Zeng, S. Liu, J. Xu, A. Zhang, Y. Song, L. Yang, A. Pu, Y. Ni and F. Chi, *J. Environ. Chem. Eng.*, 2021, **9**, 106490.

39 X. Wei, Q. Liu, H. Zhang, Z. Lu, J. Liu, R. Chen, R. Li, Z. Li, P. Liu and J. Wang, *Dalton Trans.*, 2017, **46**, 15746–15756.

40 J. Yu, H. Zhang, Q. Liu, J. Zhu, J. Yu, G. Sun, R. Li and J. Wang, *J. Hazard. Mater.*, 2022, **440**, 129735.

41 M. N. Sahmoune, *Environ. Chem. Lett.*, 2019, **17**, 697–704.

42 L. Feng, H. Wang, T. Feng, B. Yan, Q. Yu, J. Zhang, Z. Guo, Y. Yuan, C. Ma, T. Liu and N. Wang, *Angew. Chem., Int. Ed.*, 2022, **61**, 82–86.